ADVANCED MATERIALS

www.advmat.de

Iodine Vacancy Redistribution in Organic–Inorganic Halide Perovskite Films and Resistive Switching Effects

*Xiaojian Zhu, Jihang Lee, and Wei D. Lu**

Organic–inorganic halide perovskite (OHP) materials, for example, $CH_3NH_3PbI_3$ ($MAPbI_3$), have attracted significant interest for applications such as solar cells, photodectors, light-emitting diodes, and lasers. Previous studies have shown that charged defects can migrate in perovskites under an electric field and/or light illumination, potentially preventing these devices from practical applications. Understanding and control of the defect generation and movement will not only lead to more stable devices but also new device concepts. Here, it is shown that the formation/annihilation of iodine vacancies (V_I's) in $MAPbI_3$ films, driven by electric fields and light illumination, can induce pronounced resistive switching effects. Due to a low diffusion energy barrier (≈0.17 eV), the V_I's can readily drift under an electric field, and spontaneously diffuse with a concentration gradient. It is shown that the V_I diffusion process can be suppressed by controlling the affinity of the contact electrode material to I^- ions, or by light illumination. An electrical-write and optical-erase memory element is further demonstrated by coupling ion migration with electric fields and light illumination. These results provide guidance toward improved stability and performance of perovskite-based optoelectronic systems, and can lead to the development of solid-state devices that couple ionics, electronics, and optics.

The recent emergence of organic–inorganic halide perovskite materials, represented by $CH_3NH_3PbI_3$, has generated strong interest for a broad range of high-performance optoelectronic applications including solar cells,[1] photodectors,[2] light-emitting diodes,[3] and lasers.[4] Notably, devices using OHP materials as the light absorption layer can offer photoelectric conversion efficiencies of more than 20%, competing favorably with solid-state solar cells.[5,6] The superior performance can be attributed to the high optical absorption coefficient (≈10^5 cm^{-1}) with a sharp absorption edge,[7] long carrier lifetime,[8] low non-radiative carrier recombination rate,[9] and high photoluminescence (PL) quantum efficiency.[10]

The stability of OHP-based devices has been shown to be strongly affected by ion migration inside the OHP films.[11] Recent experimental studies have verified that I^- and MA^+ are mobile under an electric field,[12,13] supporting theoretical analysis results that indicate I^- (0.1–0.6 eV) and MA^+ (0.46–0.84 eV) have low activation energies for migration in $MAPbI_3$.[11,14,15] The effects of point defects including vacancies, interstitials, and (anti-)substitutions such as V_{Pb}, V_I, V_{MA}, MA_i, I_i, and MA_{Pb}, with low formation energies in $MAPbI_3$ were analyzed in a theoretical study, which showed that these point defects can form shallow defect levels in the conduction band (MA_i, V_I) and valence band (V_{Pb}, V_{MA}, MA_{Pb}, I_i) of $MAPbI_3$.[9] Consequently, accumulation of high concentrations of such shallow defects can lead to a decrease of the electric resistance of $MAPbI_3$ and produce electric-field-driven resistive switching (RS) effects.[16–18] Indeed, RS effects have recently been observed experimentally in devices based on $MAPbI_3$ films sandwiched between two electrodes.[19–22] The resistance ratio between the high-resistance state (HRS) and the low-resistance state (LRS) can reach 10^6 under an applied electric field of ≈1 V μm^{-1},[20] indicating point defects can reversibly migrate over long distances across the film, and accumulation of large amounts of defects can occur during normal device operations.

Besides electric field, light illumination has also been observed to cause defect redistribution in $MAPbI_3$ films,[23] indicating possibly strong coupling of light illumination and defect generation and movement. However, questions still remain regarding the chemical nature of the defects, and whether and how the distribution of these defects lead to the observed RS effects. In this study, we verify that the RS effects in $MAPbI_3$ films are caused by the formation/annihilation of conduction channels with high concentrations of V_I's, driven by an applied electric field and/or light illumination. The migration and accumulation of V_I's can lead to dramatic resistance changes, of over 10^7. We observed that V_I's have a low activation energy barrier (≈0.17 eV) for migration and can both readily drift under an electric field and spontaneously diffuse with a concentration gradient. We further show that the diffusion dynamics of the V_I's is strongly dependent on the affinity of I^- ions to the contact electrode material, and can also be modulated by the illumination intensity. These results verify the nature of the defect (iodine vacancy) migration behaviors in OHP materials, and provide insight into defect formation/annihilation

Dr. X. Zhu, J. Lee, Prof. W. D. Lu
Department of Electrical Engineering and Computer Science
The University of Michigan
Ann Arbor, MI 48109, USA
E-mail: wluee@eecs.umich.edu

The ORCID identification number(s) for the author(s) of this article can be found under https://doi.org/10.1002/adma.201700527.

DOI: 10.1002/adma.201700527

 © 2017 WILEY-VCH Verlag GmbH & Co. KGaA, Weinheim

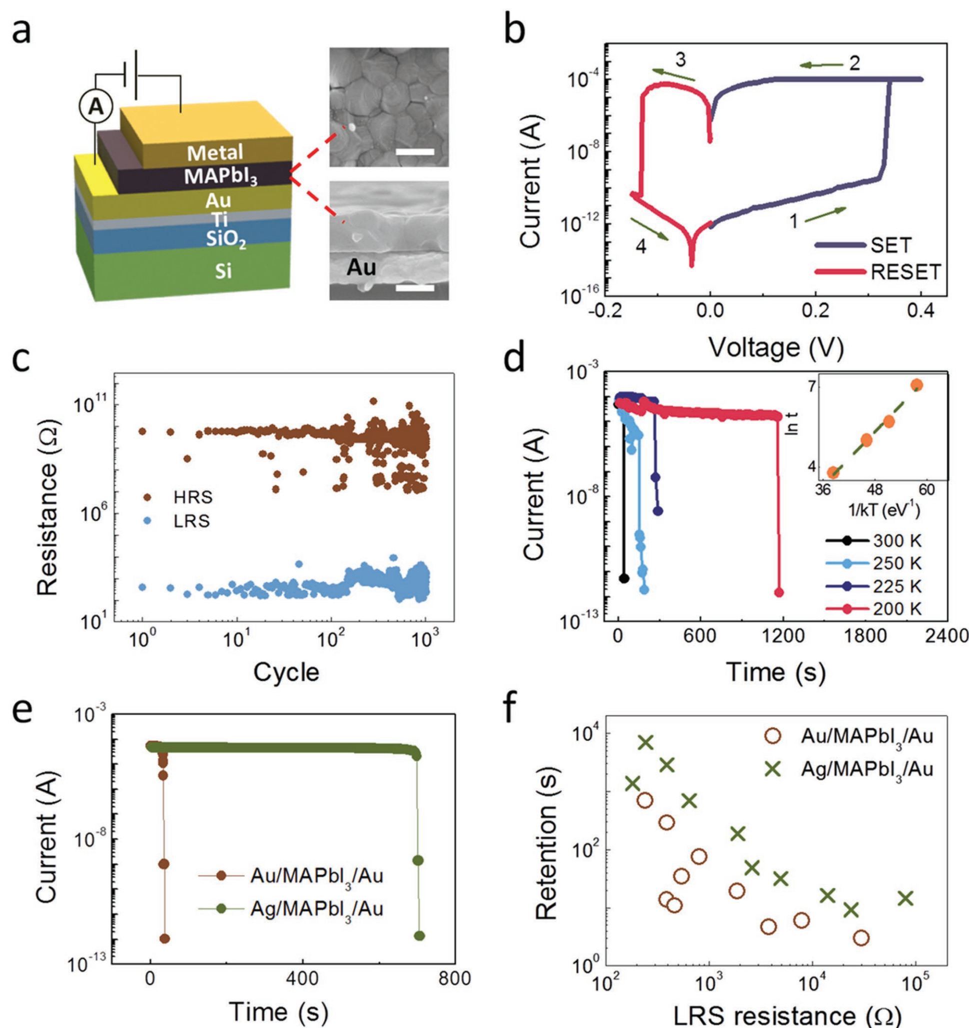

Figure 1. RS effects in $MAPbI_3$. a) Schematic of the metal/$MAPbI_3$/Au device structure, the current–voltage (*I*–*V*) measurement setup, and SEM images showing the top view (top) and side view (bottom) of the $MAPbI_3$ film. Scale bars: 200 nm. b) *I*–*V* characteristics of the Au/$MAPbI_3$/Au device during RS. During SET, a compliance current of 10^{-4} A was applied to prevent the device from hard breakdown. c) Endurance test results. The resistances at HRS and LRS were read at 0.03 V. d) Temperature-dependent LRS retention behavior. The device was SET to the same initial resistance of ≈600 Ω. A constant read bias (0.03 V) was applied to monitor the evolution of device resistance with time. Inset: $\ln(t)$–$1/kT$ plot. e) Retention behaviors of an Au/$MAPbI_3$/Au device and an Ag/$MAPbI_3$/Au device. f) Dependence of the retention time on the LRS resistance, for Au/$MAPbI_3$/Au and Ag/$MAPbI_3$/Au devices.

and redistribution processes that will help guide the implementation of OHP-based optoelectronic devices with improved stability. Additionally, new devices and applications can be developed that take advantage of the giant resistance changes in this emerging material system with efficient coupling of ionic, electronic, and photonic processes.

The $MAPbI_3$ film used in this study was deposited using a solution-based method.[24] A typical device consists of an ≈200 nm thick $MAPbI_3$ film deposited on a SiO_2/Si substrate with prefabricated Au (200 nm)/Ti (5 nm) bottom electrodes (BEs), followed by the deposition of the Au top electrodes (TEs, ≈100 nm thick with a diameter of 100 µm). Detailed experimental processes can be found in the Experimental Section. **Figure 1**a shows a schematic of the device structure, along with the current–voltage (*I*–*V*) measurement setup and scanning electron microscopy (SEM) images (top view and side view) of the deposited $MAPbI_3$ film. The as-fabricated device shows a high resistance of 1.1×10^{10} Ω (read under 0.03 V). When subjected to a positive voltage sweep (0 V → 0.4 V → 0 V, applied on the TE with the BE grounded), the device switched to a LRS at around 0.32 V with a resistance value of 1.2×10^3 Ω, that is, ≈10^7 lower than the initial state (Figure 1b). This process is termed the SET process. During the negative voltage sweep process (0 V → −0.15 V → 0 V), the device switched back to the HRS again at around −0.13 V, corresponding to the RESET process. The small shift of the minimum current location to V= −0.03 V during RESET may be attributed to the nanobattery effect caused by the inhomogeneous distribution of charged defects.[25,26] Further positive/negative voltage sweeps can repeatedly switch the device between the HRS and the LRS for over 10^3 cycles (Figure 1c), suggesting reversible bipolar RS characteristics in the $MAPbI_3$ film. Transient programming measurements show that the device can be programmed by SET/RESET voltage pulses within 400 ns (Figure S1, Supporting

© 2017 WILEY-VCH Verlag GmbH & Co. KGaA, Weinheim

Information). Additionally, the device can be switched to LRSs with different resistance values by controlling the current compliance during the SET process (Figure S2, Supporting Information), showing multilevel RS capability. The electric field that drove the SET process in our device is estimated to be in the range of 1–2 V μm^{-1}, comparable to the electric field values used to induce ion (I^- and MA^+) redistribution in $MAPbI_3$ films reported in earlier studies.[12,13]

We note that the device at LRS can spontaneously restore to HRS without applying negative RESET voltage biases. Retention failure at LRS in ionics-based RS devices can be explained by ion diffusion with a concentration gradient.[27] For example, in metal-oxide-based RS devices, the RS events are explained by the movement and redistribution of oxygen vacancies (V_O's), where a high concentration of V_O's leads to a low resistance.[17,28,29] The localized high V_O concentration regions in turn create V_O concentration gradients that can lead to spontaneous V_O diffusion and results in the retention failure at LRS.[27] Specifically, the V_O diffusion process is thermally activated and the retention time (t) has been shown to be proportional to $\exp\left(\frac{E_a}{kT}\right)$,[27] where E_a is the activation energy for ion (i.e., V_O) migration, k is the Boltzmann constant, and T is the absolute temperature. Following this model, temperature-dependent retention measurements were performed to determine the diffusion energy barrier for the species that cause RS in the $MAPbI_3$ film. Figure 1d shows the retention measurement results of an Au/$MAPbI_3$/Au device at LRS (≈600 Ω) at different temperatures. A small constant read bias (0.03 V) was applied to monitor the evolution of resistance over time. The retention time was found to increase from 44 to 1170 s when the temperature decreased from 300 to 200 K. Examining ln(t) versus $1/kT$ (inset of Figure 1d) indeed showed a linear relationship with an extracted activation energy E_a (obtained from the slope of the fitting) of 0.17 eV, consistent with the values reported for I^- ions in the form of V_I or I_i (0.1–0.6 eV),[15,23,30] suggesting that the movement of I^- ions is the dominate process that contributes to the observed RS effects.

Interestingly, replacing the Au TE (the anode during SET) with an Ag TE leads to a dramatically improved LRS retention behavior, as shown in Figure 1e. Improvement of retention time by more than one order of magnitude (from 38 to 706 s) can be observed after changing the anode material from Au to Ag (I–V curves, endurance, and switching speed test results of the Ag/$MAPbI_3$/Au RS devices are shown in Figure S3, Supporting Information). The retention behaviors were further analyzed at different LRS values, shown in Figure 1f. Increasing the LRS resistance (corresponding to a smaller conductive region at LRS) results in a decreased retention time in both devices, consistent with the ion diffusion model. In all cases, devices with Ag as the anode consistently showed an improved retention behavior. It was also found that the SET voltage of the device with Ag anode is 0.20 ± 0.07 V, lower than that of the device with Au anode (0.27 ± 0.10 V) (comparison of the RS performances in the devices with Au and Ag anodes is shown in Table S1, Supporting Information).

To directly identify the main ionic species involved in the RS process and map the ion distribution, we performed energy-dispersive X-ray spectroscopy (EDX) measurements and analyzed the elemental distributions in the $MAPbI_3$ film at the pristine state, LRS, and HRS. **Figure 2**a shows the planar Ag/$MAPbI_3$/Ag device structure used for the EDX measurement, with Figure 2b showing an SEM image of the device focusing on the $MAPbI_3$ film between the electrodes. The elemental distributions in the as-fabricated $MAPbI_3$ film at different positions were studied first. The EDX spectra collected from different positions along the film indicate uniform chemical composition with an average atomic ratio between I and Pb elements I:Pb = 2.99 ± 0.04, suggesting good stoichiometry of the as-fabricated $MAPbI_3$ film (Figure S4, Supporting Information). After applying a voltage sweep (with the electric field direction pointing to the right Ag electrode, as indicated in Figure 2 b, with compliance current of 10^{-4} A) that switched the device to the LRS with a resistance of ≈10^3 Ω (Figure S5, Supporting Information), the distributions of I:Pb at locations 1–4 along the film (marked in the SEM image in Figure 2b) were measured again. Figure 2c (left) shows the collected EDX spectra of the main characteristic X-ray peaks for Pb (Mα: 2.36 keV and Mβ: 2.44 keV) and I (Lα: 3.95 keV, Lβ_1: 4.24 keV, Lβ_2: 4.52 keV, and Lγ_1: 4.84 keV). Note that the spectra have been normalized against the intensity of the characteristic Pb M series peaks. Examination of the I spectra at different locations (Figure 2c, right) shows that the I intensity gradually decreased from locations 1 to 4. Quantitative analysis of the I:Pb ratio (Figure 2d) shows that from 1, 2, 3 to 4, the I:Pb ratio gradually decreased from 2.76, 2.28, 1.42 to 1.01, respectively, along the electric field direction applied during RS. Control studies obtained from another device switched by a bias direction pointing to the left Ag electrode (Figure S6, Supporting Information) confirmed that the I:Pb ratio is always reduced along the electric field direction after RS. Note that the migration of Ag into $MAPbI_3$ film from the anode was only occasionally observed when the device was programmed to LRS under high compliance current (≥8 mA) (Figure S7, Supporting Information). At the much lower SET compliance current (≤0.1 mA) conditions used in this work, formation of Ag filaments can be ruled out. This observation was further supported by the semiconducting behavior of the device at LRS (Figure S8, Supporting Information) vs. metallic behavior expected from an Ag-based filament.

Based on the much lower activation energy for I^- migration (0.1–0.6 eV) compared to Pb^{2+} migration (0.8–2.3 eV) from earlier theoretic calculations[11,14,15,31] as well as previous experimental results[12,32] and our own retention measurements that suggested low diffusion energy barrier of I^- ions, the observed changes in the I:Pb ratio is attributed to the migration of I^- ions under the electric field during RS. Additionally, the fact that the I:Pb ratio is below the stoichiometry value of 3 throughout the $MAPbI_3$ film, and significantly below the stoichiometry value near the cathode (I:Pb = 1.01 at location 4) suggests the specific ionic species involved in the RS process should be V_I's rather than I_i's. We note that due to the limited spatial resolution of element mapping in EDX measurements, the obtained I:Pb value is an averaged one and the actual V_I concentration in localized regions may be even higher. This explanation is consistent with previous findings that show V_I's can act as donors that form a shallow defect level in the conduction band of $MAPbI_3$,[9] thus regions with high concentrations of V_I's can act as conducting

© 2017 WILEY-VCH Verlag GmbH & Co. KGaA, Weinheim

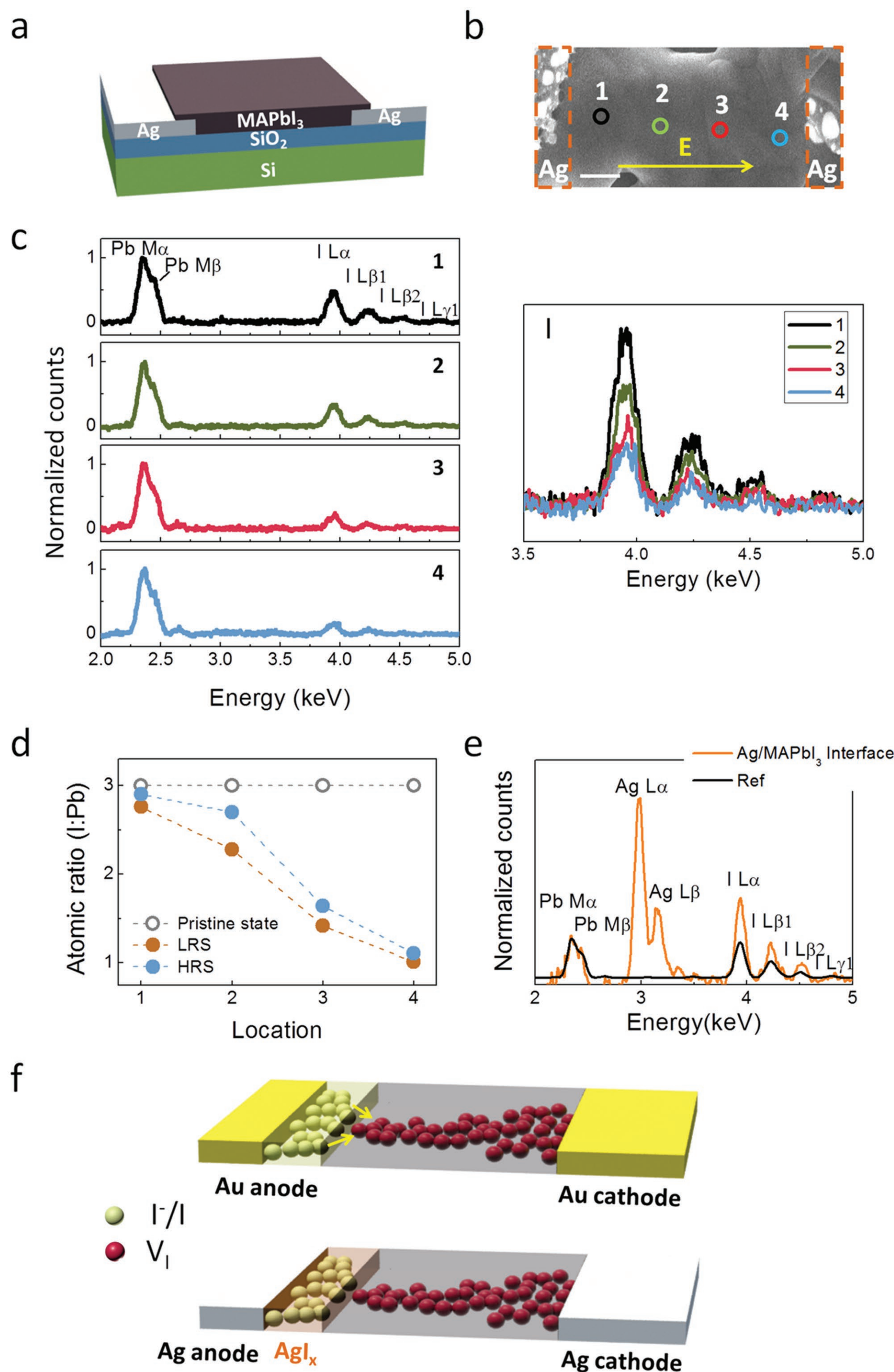

Figure 2. EDX analysis of elemental distributions in Ag/$MAPbI_3$/Ag devices. a) Schematic of the device structure for EDX characterization. b) SEM image of the device. Locations 1–4 mark the positions where the EDX analyses were performed. The arrow shows the electric field direction during SET. The dashed lines mark the locations of the Ag electrodes. Scale bar: 300 nm. c) Left: EDX spectra of the device at LRS, showing the main characteristic X-ray peaks of Pb (M series) and I (L series) collected at locations 1–4 in (b). The spectra have been normalized against the intensity of the characteristic Pb M series peaks. Right: Comparison of the I peaks at locations 1–4. d) Quantitative atomic concentration ratio between I and Pb at locations 1–4 at the pristine, LRS, and HRS states. e) EDX spectrum showing the Pb, Ag, and I characteristic X-ray peaks at the Ag (anode)/$MAPbI_3$ interface. The spectrum of the stoichiometric $MAPbI_3$ film, which has been normalized against the intensity of Pb peaks, is shown for reference. f) Schematics showing the hypothesized I^- ion storage and diffusion processes. The conductive channel is formed by the high V_I concentration region.

 © 2017 WILEY-VCH Verlag GmbH & Co. KGaA, Weinheim

channels and lead to switching from HRS to LRS. We note that at the anode/$MAPbI_3$ interface the I:Pb ratio can reach to almost ≈5 at some locations, along with pronounced presence of Ag. A representative spectrum is shown in Figure 2e, suggesting the accumulation of I^- ions at the anode/$MAPbI_3$ interface. This observation may help explain the electrode material dependent LRS retention behavior, and provide additional insight into the V_I generation and migration process. During the RS process from HRS to LRS, the I^- ions are attracted to the anode and can be potentially stored inside the electrode material. This process creates V_I's in the $MAPbI_3$ film, with the highest V_I concentration (lowest I:Pb ratio) near the cathode. Continued application of the voltage bias will cause the expansion of V_I-rich regions toward the anode and eventually form a conduction channel bridging the electrodes, as schematically shown in Figure 2f. Previous studies on I^- ion adsorption on Au films have suggested that I^- ions can be stored in the Au film in the form of neutral I atoms at low anodic potentials (≈0.4 V).[33] At high anodic potentials (>0.8 V) complexes like AuI_2^-/AuI_4^- may also form where Au atoms from the electrode may be dissolved to form Au^+/Au^{3+}.[34] Considering the low voltages (≤0.4 V) used in our devices, the adsorbed I^- ions will most likely be in elemental I form. In this case, after removing the bias voltage the stored I atoms can spontaneously diffuse outside of the Au electrode and recombine with the V_I's in the $MAPbI_3$ film, leading to rupture of the conductive channels and retention failure. In contrast, in devices with Ag anodes, the electrochemically active Ag electrode[35] can react with the stored I^- ions and act as an effective I^- ion reservoir layer through the formation of AgI_x, thus suppressing the diffusion of I^- ions from the electrode region and the recombination process with V_I's in the $MAPbI_3$ film. The half-cell reactions at the anode in the devices using Au and Ag anode can be expressed as

$$\text{Au anode}: I^- \leftrightarrow I + e^- \quad (1)$$

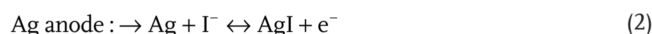

$$\text{Ag anode}: \rightarrow Ag + I^- \leftrightarrow AgI + e^- \quad (2)$$

This hypothesis also explains the lower SET voltage observed in devices with Ag anode (Table S1, Supporting Information), since the electrode reduction potential of $E^0(AgI/I^-)$ (−0.15224 V)[36] is lower than that of $E^0(I_2/I^-)$ (0.54 V)[37] thus the formation of AgI_x in Ag anode requires a lower anodic potential than the formation of elemental I in Au anode. This hypothesis successfully explains the observed RS behavior and the electrode dependence, and is consistent with models used for oxide-based RS devices that have been widely accepted by the research community.[38,39] After applying a negative bias voltage to switch the device to the HRS, the I:Pb ratios at locations 1–4 increased to 2.87, 2.7, 1.64 and 1.11 respectively (Figure 2d and Figure S9, Supporting Information). Specifically, the I:Pb ratios at locations 1 and 2 became close to the stoichiometric value of 3 after RESET, supporting the proposed mechanism that the I^-s stored in the Ag electrode migrate into the $MAPbI_3$ film during the RESET process and the RS effect occurs near the Ag/$MAPbI_3$ interface.

To verify the hypothesis, we further performed depth profile characterization of the Ag chemical states in devices with Ag anodes, through the X-ray photoelectron spectroscopy (XPS) technique. **Figure 3**a shows the schematic of the vertical Ag/$MAPbI_3$/Au device structure used in the XPS measurement setup. During the Ar ion etching process, the Ar pressure was carefully maintained and the etching rate of Ag was fixed at ≈4 nm min^{-1}. Each etching step lasted for 3 min, corresponding to an etching thickness of about 12 nm. We first analyzed the depth profile of the chemical state of Ag in the as-fabricated device as a control sample. Figure 3b shows the Ag 3d XPS spectra collected from different depths in the Ag electrode after timed Ar etch. After an initial surface cleaning process for 6 min, the collected spectrum (≈76 nm above the Ag/$MAPbI_3$ interface) exhibited two main peaks located at around 374.1 and 368.1 eV, corresponding to the Ag^0 $3d_{3/2}$ and Ag^0 $3d_{5/2}$ peaks, respectively.[40] No apparent transition of the peak positions was observed following the Ar etching processes at different depths, suggesting that the metallic characteristics of the Ag electrode apparently did not change in the device. On the contrary, for the device switched to LRS (Figure 3c, ≈200 Ω), a clear shift of the peak positions to lower binding energies by ≈0.4 eV was observed starting from etching time = 15 min (≈40 nm above the Ag/$MAPbI_3$ interface), with the new peak positions located at 373.7 and 367.7 eV, respectively, suggesting oxidization of the Ag electrode. The peak positions were maintained until the Ag/$MAPbI_3$ interface was reached (at etching time = 24 min), consistent with the hypothesis that the oxidization of Ag started from the Ag/$MAPbI_3$ interface and extended into the Ag electrode. The oxidized Ag signals are attributed to the formation of AgI_x, since the new peak positions are consistent with the Ag^+ 3d peak positions in AgI[41] and the transition region starts from the bottom of the Ag electrode that is in direct contact with the $MAPbI_3$ film and extends ≈40 nm into the Ag electrode. The Ag iodization hypothesis is further supported by the observation of I^- 3d peaks (I^- $3d_{3/2}$: 630.6 eV and I^- $3d_{5/2}$: 619.1 eV[42]) in the spectrum collected in the Ag layer near the Ag/$MAPbI_3$ interface in the device at LRS (Figure 3d). Such I peaks were not observed in the as-fabricated device. These XPS results are consistent with the EDX results shown in Figure 2e and support the hypothesis that the Ag electrode acts as I^- reservoir during the SET process through the formation of stable AgI_x.

Studies were then performed on how light illumination can affect the ionic migration processes in $MAPbI_3$. **Figure 4**a shows the schematic of the Ag/$MAPbI_3$/Au planar device structure used to study the effect of light illumination. Broadband visible light with different intensities (from 0 to 1.29 μW cm^{-2}) were used in this study. As shown in Figure 4b, during SET the voltage required to switch the device steadily increased from 2.1, 2.3, 2.5, 2.7, 3.1 to 3.8 V when the illumination intensity was increased from 0, 0.03, 0.19, 0.38, 0.73 to 1.29 μW cm^{-2}. The relationship between the SET voltage and illumination intensity is shown in Figure 4c, highlighting the increase in SET voltage with increased illumination intensity. On the other hand, after programming the device to LRS in the dark, the voltage required to RESET the device was found to decrease with increased illumination intensity (Figure 4d,e). Further measurements showed that illumination with a high intensity laser (4–12 mW cm^{-2}, 525 nm) can lead to further increased SET voltages (Figure S10, Supporting Information) and fast LRS retention failure (Figure 4f). These results suggest that

© 2017 WILEY-VCH Verlag GmbH & Co. KGaA, Weinheim

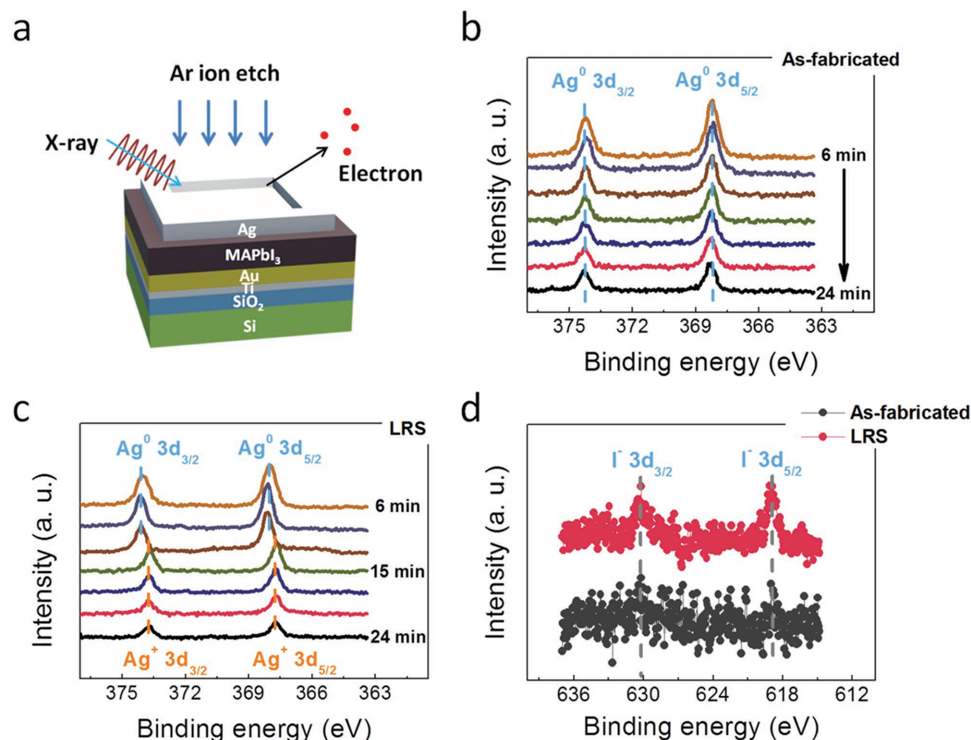

Figure 3. Depth profile analysis of the Ag and I chemical states. a) Schematic of the device structure and the XPS measurement setup. Each spectrum is collected after timed Ar ion etching process. b,c) XPS depth profiles of the Ag^0/Ag^+ 3d peaks in the b) as-fabricated device and c) device at LRS. d) XPS spectra of I^- 3d peaks obtained in the Ag electrode layer near the $Ag/MAPbI_3$ interface, for as-fabricated device and device at LRS.

light illumination will inhibit the formation (and facilitate the annihilation) of V_I-rich conductive paths in the $MAPbI_3$ film. This finding is consistent with results obtained from PL measurements of $MAPbI_3$,[23,30] which showed that V_I^+ in $MAPbI_3$ under light illumination is unstable and will spontaneously diffuse and combine with I_i^-. Since V_I^+'s act as nonradiative recombination centers, increases of the PL lifetime and the PL intensity were observed in measurements under light illumination, with higher illumination intensity resulting in stronger effects.[23]

Finally, we note the ability to control ion migration in $MAPbI_3$, using both an applied electric field and light illumination, can potentially lead to coupled electronic, ionic, and photonic devices. Figure 4g shows one such example, where an electrical-write and optical-erase memory element with reversible resistance changes up to seven orders of magnitude was demonstrated by alternatively applying an electrical bias (which SETs the device) and light illumination (which RESETs the device) (Figure S11, Supporting Information). Light interaction with the device can allow information stored in the memory to be remotely controlled by light, and also suggests that the memory at LRS can be used to qualitatively analyze light intensity information since high-intensity light can switch the device to HRS whereas low-intensity light does not affect the resistance state.

In summary, we show the migration and redistribution of V_I's can lead to the formation/annihilation of conductive channels and result in dramatic resistance changes in $MAPbI_3$. A low diffusion energy barrier of ≈0.17 eV was obtained for V_I's. The spontaneous diffusion of I^- ions that lead to retention loss can be suppressed by using an active anode (e.g., Ag to form stable AgI_x at the electrode/$MAPbI_3$ interface). From the perspective of optoelectronic applications, the formation of ionic defects due to ion migration is detrimental since it may not only affect device stability but also potentially induce short circuit problems due to formation of conduction channels. Systematic engineering of the material property including the electrode/OHP interface or illumination conditions can potentially address these concerns. On the other hand, these emerging materials with low activation energy for ion migration may provide opportunities to develop high-speed solid-state devices that can efficiently couple ionic, electronic, and photonic effects at the individual device level. Beyond the OHP material system, we believe that RS effects can be used to reveal ion migration in a broad range of semiconductors and help gain insight into the ion redistribution behaviors at the nanoscale.

Experimental Section

Device Fabrication: The bottom Au/Ti (200 nm/5 nm) electrode was first deposited on a SiO_2/Si wafer by photolithography, e-beam evaporation, and liftoff processes. The sample was then treated by oxygen plasma for 5 min before spin-coating the $MAPbI_3$ film. Precursor solution with a concentration of 40 wt% was prepared by mixing weighted $MAPbI_3$ powders (99.5%, Borun New Material Technology Co., Ltd.) in *N*,*N*-dimethylformamide (DMF, 99.8%, Sigma-Aldrich), and stirred at 70 °C for 2 h. To produce a uniform $MAPbI_3$ film, the precursor solution was spin-coated on the Au/Ti/SiO_2/Si substrate at 4000 rpm for 60 s, during which a small amount of toluene (99.8%, Sigma-Aldrich) was dropped

 © 2017 WILEY-VCH Verlag GmbH & Co. KGaA, Weinheim

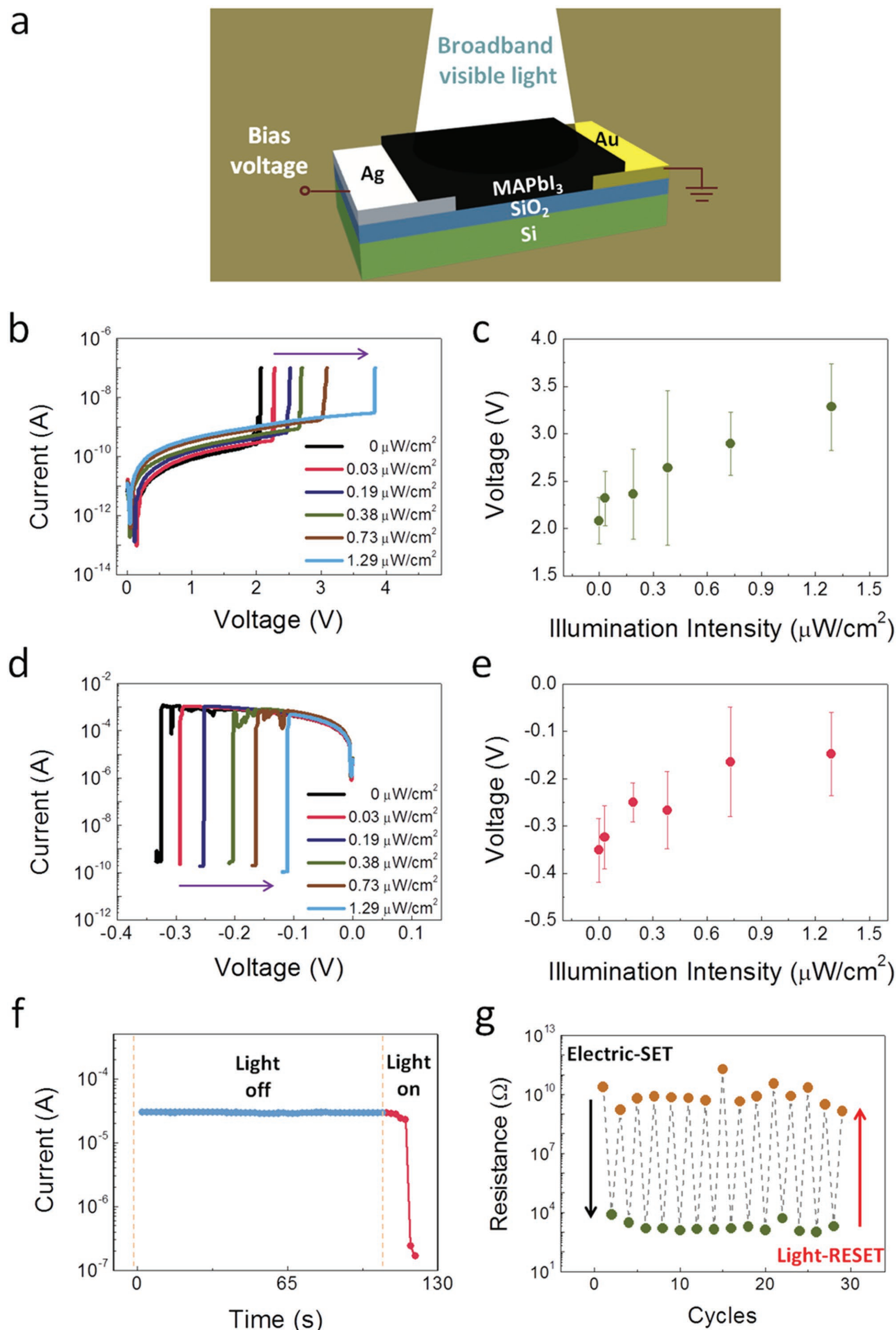

Figure 4. V_I dynamics affected by light illumination. a) Schematic of the device structure. The device is exposed to broadband visible light with intensity from 0 to 1.29 µW cm^{-2}. Effects of illumination on the b) SET process and d) RESET process with different illumination intensities. Dependence of the c) SET voltage and e) RESET voltage on illumination intensity. f) Evolution of the device resistance (measured under 0.1 V) in the device at LRS. The device was measured in the dark in the first 105 s, followed by light illumination (4 mW cm^{-2}, 525 nm). g) Cycling of the LRS and HRS with electric-SET and light-RESET, demonstrating the device reliability.

on the substrate center at 6–8 s. The sample was then transferred to a hot plate at 75 °C and annealed for 20 min. Finally, the Au and Ag metal electrodes (100 µm in diameter) were deposited on the $MAPbI_3$ film by e-beam evaporation through a stainless steel shadow mask.

Measurements: Electric characterizations were performed with a Keithley 4200s semiconductor parameter analyzer system in a variable temperature probe station. SEM images and EDX spectra of the devices were acquired from a Hitachi SU8000 system at 10 kV with emission

© 2017 WILEY-VCH Verlag GmbH & Co. KGaA, Weinheim

current 7 µA. XPS characterizations were performed with a Kratos Axis Ultra system with a monochromated Al anode. The source was operated at 14 kV with emission current 8 mA. To minimize the possible diffusion of Ag or I at the Ag/$MAPbI_3$ interface, the electrical measurements and XPS characterizations were carried out within 24 h after the device fabrication. The broadband visible light was created by a halogen lamp. The monochromatic light (525 nm) was created by a laser source (Uniphase, Green-SLM Laser).

Supporting Information

Supporting Information is available from the Wiley Online Library or from the author.

Acknowledgements

The authors would like to thank Dr. Chao Du for useful discussions. This work was supported in part by the AFOSR through MURI grant FA9550-12-1-0038, and by the National Science Foundation (NSF) through grant CCF-1617315.

Conflict of Interest

The authors declare no conflict of interest.

Keywords

illumination, iodine vacancy, organic–inorganic halide perovskite, resistive switching

Received: January 25, 2017
Revised: March 27, 2017
Published online: June 5, 2017

[1] M. A. Green, A. Ho-Baillie, H. J. Snaith, *Nat. Photonics* **2014**, *8*, 506.
[2] L. Dou, Y. Yang, J. You, Z. Hong, W.-H. Chang, G. Li, Y. Yang, *Nat. Commun.* **2014**, *5*, 5404.
[3] H. Cho, S.-H. Jeong, M.-H. Park, Y.-H. Kim, C. Wolf, C.-L. Lee, J. H. Heo, A. Sadhanala, N. Myoung, S. Yoo, S. H. Im, R. H. Friend, T.-W. Lee, *Science* **2015**, *350*, 1222.
[4] H. Zhu, Y. Fu, F. Meng, X. Wu, Z. Gong, Q. Ding, M. V. Gustafsson, M. T. Trinh, S. Jin, X. Y. Zhu, *Nat. Mater.* **2015**, *14*, 636.
[5] S. D. Stranks, H. J. Snaith, *Nat. Nanotechnol.* **2015**, *10*, 391.
[6] T. M. Brenner, D. A. Egger, L. Kronik, G. Hodes, D. Cahen, *Nat. Rev. Mater.* **2016**, *1*, 15007.
[7] P. Löper, M. Stuckelberger, B. Niesen, J. Werner, M. Filipič, S.-J. Moon, J.-H. Yum, M. Topi , S. De Wolf, C. Ballif, *J. Phys. Chem. Lett.* **2015**, *6*, 66.
[8] D. W. de Quilettes, S. M. Vorpahl, S. D. Stranks, H. Nagaoka, G. E. Eperon, M. E. Ziffer, H. J. Snaith, D. S. Ginger, *Science* **2015**, *348*, 683.
[9] W.-J. Yin, T. Shi, Y. Yan, *Appl. Phys. Lett.* **2014**, *104*, 063903.
[10] F. Deschler, M. Price, S. Pathak, L. E. Klintberg, D.-D. Jarausch, R. Higler, S. Hüttner, T. Leijtens, S. D. Stranks, H. J. Snaith, M. Atatüre, R. T. Phillips, R. H. Friend, *J. Phys. Chem. Lett.* **2014**, *5*, 1421.
[11] Y. Yuan, J. Huang, *Acc. Chem. Res.* **2016**, *49*, 286.
[12] Y. Yuan, Q. Wang, Y. Shao, H. Lu, T. Li, A. Gruverman, J. Huang, *Adv. Energy Mater.* **2016**, *6*, 1501803.
[13] Y. Yuan, J. Chae, Y. Shao, Q. Wang, Z. Xiao, A. Centrone, J. Huang, *Adv. Energy Mater.* **2015**, *5*, 1500615.
[14] C. Eames, J. M. Frost, P. R. F. Barnes, B. C. O'Regan, A. Walsh, M. S. Islam, *Nat. Commun.* **2015**, *6*, 7497.
[15] J. M. Azpiroz, E. Mosconi, J. Bisquert, F. De Angelis, *Energ. Environ. Sci.* **2015**, *8*, 2118.
[16] R. Waser, R. Dittmann, G. Staikov, K. Szot, *Adv. Mater.* **2009**, *21*, 2632.
[17] Y. Yang, W. Lu, *Nanoscale* **2013**, *5*, 10076.
[18] J. J. Yang, D. B. Strukov, D. R. Stewart, *Nat. Nanotechnol.* **2013**, *8*, 13.
[19] E. J. Yoo, M. Lyu, J.-H. Yun, C. J. Kang, Y. J. Choi, L. Wang, *Adv. Mater.* **2015**, *27*, 6170.
[20] J. Choi, S. Park, J. Lee, K. Hong, D.-H. Kim, C. W. Moon, G. D. Park, J. Suh, J. Hwang, S. Y. Kim, H. S. Jung, N.-G. Park, S. Han, K. T. Nam, H. W. Jang, *Adv. Mater.* **2016**, *28*, 6562.
[21] C. Gu, J.-S. Lee, *ACS Nano* **2016**, *10*, 5413.
[22] E. Yoo, M. Lyu, J.-H. Yun, C. Kang, Y. Choi, L. Wang, *J. Mater. Chem. C* **2016**, *4*, 7824.
[23] D. W. deQuilettes, W. Zhang, V. M. Burlakov, D. J. Graham, T. Leijtens, A. Osherov, V. Bulovi , H. J. Snaith, D. S. Ginger, S. D. Stranks, *Nat. Commun.* **2016**, *7*, 11683.
[24] M. Xiao, F. Huang, W. Huang, Y. Dkhissi, Y. Zhu, J. Etheridge, A. Gray-Weale, U. Bach, Y.-B. Cheng, L. Spiccia, *Angew. Chem., Int. Ed.* **2014**, *126*, 10056.
[25] I. Valov, E. Linn, S. Tappertzhofen, S. Schmelzer, J. van den Hurk, F. Lentz, R. Waser, *Nat. Commun.* **2013**, *4*, 1771.
[26] S. Tappertzhofen, E. Linn, U. Böttger, R. Waser, I. Valov, *IEEE Electron Dev. Lett.* **2014**, *35*, 208.
[27] S. Choi, J. Lee, S. Kim, W. D. Lu, *Appl. Phys. Lett.* **2014**, *105*, 113510.
[28] J.-Y. Chen, C.-W. Huang, C.-H. Chiu, Y.-T. Huang, W.-W. Wu, *Adv. Mater.* **2015**, *27*, 5028.
[29] I. Goldfarb, F. Miao, J. J. Yang, W. Yi, J. P. Strachan, M. X. Zhang, M. D. Pickett, G. Medeiros-Ribeiro, R. S. Williams, *Appl. Phys. A* **2012**, *107*, 1.
[30] E. Mosconi, D. Meggiolaro, H. J. Snaith, S. D. Stranks, F. De Angelis, *Energy Environ. Sci.* **2016**, *9*, 3180.
[31] J. Haruyama, K. Sodeyama, L. Han, Y. Tateyama, *J. Am. Chem. Soc.* **2015**, *137*, 10048.
[32] C. Li, S. Tscheuschner, F. Paulus, P. E. Hopkinson, J. Kießling, A. Köhler, Y. Vaynzof, S. Huettner, *Adv. Mater.* **2016**, *28*, 2446.
[33] B. G. Bravo, S. L. Michelhaugh, M. P. Soriaga, I. Villegas, D. W. Suggs, J. L. Stickney, *J. Phys. Chem.* **1991**, *95*, 5245.
[34] B. H. Loo, *J. Phys. Chem.* **1982**, *86*, 433.
[35] Y. Yang, P. Gao, S. Gaba, T. Chang, X. Pan, W. Lu, *Nat. Commun.* **2012**, *3*, 732.
[36] P. W. Atkins, *Physical Chemistry*, 6th ed., Freeman, New York **1997**.
[37] V. Petr, *Handbook of Chemistry and Physics*, CRC Press, Boca Raton, FL, USA **2012**.
[38] L. Goux, A. Fantini, Y. Y. Chen, A. Redolfi, R. Degraeve, M. Jurczak, *ECS Solid State Lett.* **2014**, *3*, Q79.
[39] Y. Y. Chen, M. Komura, R. Degraeve, B. Govoreanu, L. Goux, A. Fantini, N. Raghavan, S. Clima, L. Zhang, A. Belmonte, A. Redolfi, G. S. Kar, G. Groeseneken, D. J. Wouters, M. Jurczak, *IEDM Technol. Dig. IEEE* **2013**, 252.
[40] G. Schon, *Acta Chem. Scand.* **1973**, *27*, 2623.
[41] Y. Liang, H. Wang, L. Liu, P. Wu, W. Cui, J. G. McEvoy, Z. Zhang, *J. Mater. Sci.* **2015**, *50*, 6935.
[42] Y. Kato, L. K. Ono, M. V. Lee, S. Wang, S. R. Raga, Y. Qi, *Adv. Mater. Interfaces* **2015**, *2*, 1500195.

© 2017 WILEY-VCH Verlag GmbH & Co. KGaA, Weinheim